Reactions of RPV Nozzle Corner Areas to Loads Consistent with Operational and Accident Conditions

K. Kussmaul, J. Jansky, P. Pfeffer, S. Krolop
Staatliche Materialprüfungsanstalt (MPA), Universität Stuttgart, Pfaffenwaldring 32, D-7000 Stuttgart 80, Germany
W. Schmitt
Fraunhofer-Institut für Werkstoffmechanik, Wöhlerstr. 11, D-7800 Freiburg, Germany
D. Beukelmann
Technische Überwachungs-Verein Bayern e.V., Postfach 21 04 20, D-8000 München 21, Germany

Abstract

The loading of nozzle areas of a reactor pressure vessel due to normal operating conditions, cold pressure test, water side and steam side blowdown, and thermal shock was investigated theoretically and experimentally on the HDR reactor pressure vessel (OD = 2980 mm, wall thickness = 112 mm).

For the nozzles with and without cracks under different loads the cold pressure test does not represent the most severe loading case compared with the case of water side blowdown and thermal shock loading.

The comparisons of the deformations and displacements obtained at the various load levels namely for homogeneous nozzles and of CTOD- or CMOD-values, for nozzle areas affected by cracking show that extremely large safety margins exist in respect of incipient crack formation.

The pre-test evaluation of the pressurized thermal shock test series is discussed in more detail. Based on the real crack geometry (as measured by non - destructive examination) a three-dimensional, elastic-plastic finite element analysis was employed to calculate the distribution of K and J along the crack front. The loading was internal pressure and the temperature fields obtained from a three-dimensional temperature field analysis, compared with measurements.

The agreement between prediction and experiment could be improved by this analysis mainly for the extension of the crack in depth direction. However, the analysis predicted a propagation at the surface in the cladding much higher than actually observed in the test.

The value of the crack tip opening displacement is obtained from linear extrapolation of the crack edges towards the crack tip. For comparison purposes the stress intensity K is obtained both by the displacement method and from the energy release rate or J.

A safety assessment is made by comparing the fracture mechanic parameters obtained theoretically with different material characteristics from laboratory tests.

1. Introduction

In the context of the HDR safety program loading tests corresponding to test and operating conditions of a boiling water RPV were carried out on a vessel of 23 NiMoCr 3 6 cladded with X 10 CrNiNb 18 9, figure 1, /1, 2/. In addition, some nozzle areas were loaded from inside by a cyclic thermal shock transient of ΔT = 265 K under operating conditions of p = 110 bar, T = 310 °C, 8 ppm O_2 in pressurized water, /3/. Exemplary the test results determined on pressure vessel nozzle A2 with ID = 200 mm, figure 2, and several numerical and experimental results so far obtained are discussed here.

2. Results of the strain measurements

In the area of the A2 nozzle corner strain measurements with weldable strain gauges were carried out in the longitudinal and circumferential directions, /4/. On the assumption that measured strains were in principal directions the equivalent strains were calculated according to von Mises for various loading conditions with internal pressure prevailing at the time of measurement are shown in figure 3. The lowest equivalent strain at the nozzle corner was measured under operating conditions. Blowdown loading of the nozzle corner following a double-ended break of the recirculation loop (feedwater-side blowdown) causes increase of the equivalent strain by a factor of 1.5. In nozzle area S (compare fig. 1; not documented further in this report) which was directly affected by this blowdown the equivalent strain amounted to about 0.3 %. The loading during hydrostatic pressure test (p = 156 bar) is more severe and hence covers the two preceding load situations in terms of safety. The thermal shock loading of the nozzle corner surface with ΔT = 265 K leads to equivalent strains of 0.7 %. In the case of a nonincipiently cracked component (ductile material) stress relief takes place by plastification processes. The loading has then to be classed as fatigue one and verified with incipient crack curves. In the case of nozzle containing a incipient crack, the hydrostatic pressure test doesn't cover the thermal shock transient deformation on the crack tip /5/.

3. Results of crack opening measurements

After about 2900 thermal shock cycles two types of crack, figure 4, developed in the nozzle corner area. In the cylindrical region of the nozzle there are longitudinal cracks formed between the individual cladding layers. In the nozzle circumference numerous short circumferentially directed incipients cracks developed between the cladding layers welded manually and mechanically.

The longitudinal cracks in the nozzle showed preferential growth in depth, which was desired by the choice of cooling. A crack selected in the 270° degree position on the nozzle circumference was instrumented with COD transducers during the various blowdown tests. The position of the crack in the longitudinal direction of the nozzle and relative to the nozzle corner is depicted in figure 5. At positions 50, 80 and 100 mm from the nozzle corner the crack opening behaviour was measured. On completion of the blowdown and thermal shock tests this particular crack was cut out of the nozzle corner and examined fractographically. Identificable is the semi-elliptical form of the crack which has developed due to cyclic thermal transients. In the area of the cladding the crack flanks run perpendicular to the cooled surface.

As an example the crack opening and temperature measurements for a water blowdown are shown in figure 6. With falling temperature in the RPV (ΔT = 142 K) the measured CMOD values increase to about 0.06 mm. On attainment of temperature equalization the crack flanks close again; crack regions of less depth showed a tendency to lower crack opening values. Since during the blowdown the internal pressure in the RPV was lowered from 70 bar to 1 bar it can be concluded from the data obtained that internal pressure has minor effect on the crack opening range.

4. Crack propagation calculation

The crack opening is definitely determined by the duration and the temperature difference of the cooling. This is made clear in figure 7 which shows the temperature distribution calculated across the nozzle wall (cooling time up to 120 s). The more prolonged the cooling the deeper are the wall regions reached by the cooling and hence also subjected to thermal loading.

For a detailed finite element analysis the crack was modelled following a non-destructive evaluation at an intermediate test stage. The thermal part of the loading during one cooling cycle was obtained by a three dimensional finite element analysis where it was attempted to model the complete initial and boundary value problem. The temperature field obtained is in reasonable agreement with thermalcouple measurements at a nozzle surface. The crack tip loading is expressed by the variation of the J-integral along the crack front for different times into the transient (Figure 8 /6/). The maximum value of J is about 50 N/mm, the curve for t = 0 s represents the case of pure pressure loading. The J-values are particularly high in the area of the surface (path 1 and 8) only at later times into the transient the absolute maximum of J occurs at position 3. Figure 9 shows the variation of the J-integral at different crack tip positions with time. It is evident that for all internal positions (2-7) J seems to continue to increase also after 120 s. At the surface position 1 and 8 however, there is only little increase in J after 40 s. That means that the crack tip loading in the surface area cannot be increased by an increase in cooling time.

The results of the three-dimensional FE-analysis presented here in conjunction with the ASME-XI crack propagation curves led to the crack form prediction shown in figure 10 in comparison with the ultimate crack form determined fractographically. The agreement in terms of ultimate crack depth is clearly recognizable although the initial crack form was over-estimated in depth. The crack length, was greatly over-estimated in the calculation. The manner in which the material characteristic affects the precalculated crack growth can be seen for a nozzle corner crack (middle of crack length) under the same thermal shock loading in figure 11. The analysis has been performed only for the depth propagation of a nozzle corner crack between the cladding/ferrite interface (a = 8 mm) and a crack depth of 50 mm.

The crack propagation rates obtained under the same conditions (O_2 -content, loading frequency, HDR-RPV material) but on different CT specimens are higher for narrow CT specimens than for thicker. Thus, taking the characteristics of the CT 25 specimen, a crack depth of 50 mm is attained theoretically after about 250 cycles, whilst from the values of the CT 50 specimen 500 load cycles can be expected. More conservative extrapolation of the same measured laboratory values point to about 1500 load cycles for the same crack extension. An estimate made with ASME-XI crack propagation rates suggests attainment of the 50 mm depth only after 2500 cycles. Finally, extrapolation of the measured crack depth attained after 1200 cycles towards 50 mm allows the cautious estimate that about 2000 cycles are needed in the 180° position and 3400 Cycles in the 270° position (compare fig. 4). There is evidence of greater conservativeness (over-estimating of the crack propagation) in the values obtained under laboratory conditions.

The real crack propagation rates are influenced also by the crack channel disposition in the wall thickness. As shown in figure 12 the crack channel removed from the HDR nozzle corner is branched. The branching yields to a lowering of the stress intensity in a ratio of $1/\sqrt{n}$ (n = number of subcracks) /7, 8/ which causes a 30 % reduction when there are two crack channels. Hence the precalculated crack tip loads are correspondingly reduced and lead to lower crack propagation rates.

5. Safety evaluation for the HDR thermal shock

5.1 K-concept

Nozzle corner cracks were assumed to be the most serious of all possible crack forms in the nozzle area. In three-dimensional analyses the elastic K_I-values were determined for different crack depths under internal and thermal shock loading and compared with the K_I -values converted from J-values, figure 13 /9/. The limiting material values are already exceeded between crack depths of 20 and 50 mm (around 30 mm).

5.2 CTOD-concept

In comparison with critical crack opening the CTOD values calculated in 3D elastoplastic analyses reveal transgression of the limiting values already for 20 mm deep crack, figure 14. Since the actual crack developments in the nozzle corner reached already a depth of 30 mm, and no stable crack growth was observed during the tests, it can be assumed that calculation results are too conservative. This conservatism reflects the linear extrapolation methods used for estimation of CTOD-values from calculated flank angles. It has further to be taken into consideration that the critical values obtained from CT specimens were determined under extremely conservative conditions (plane strain). This is not corresponding to the actual conditions (more plane stress) /10/. According to figure 14 a crack depth of 100 mm in the nozzle corner leads already to crack initiation under loading by internal pressure only (p = 110 bar).

5.3 Constraint concept

Figure 15 shows the constraint /11/ (defined as the ratio of σ_V and σ_1) for a CT 100 specimen calculated elastoplastically and loaded until fracture occurred. For comparison the calculated constraint values for the nozzle are shaded. The CT specimen and the nozzle are made of approximately the same material. It is evident that the nozzle corner crack has a significantly lower triaxiality than the CT-specimen in terms of crack tip loading (K_{IJ} or J). The nozzle area would exhibit a higher material resistance to crack initiation and propagation.

6. Conclusion and summary

The results shown here indicate that

* the cold pressure test does not have the desired safety function for incipiently cracked nozzle corners under thermal shock loading
* the theoretical analyses of nozzle corner loading agree well with the experimental data to the stage of stress determina- tion
* calculation of the crack propagation is conservative. The agreement is good in the depth direction, but not sufficiant /satisfactory for the length direction. The crack tip in the component is branched and thus lower crack tip loading than calculated for

a single crack channel

* the crack propagation rates determined from CT specimens are different from those established in the component.

The safety analysis revealed conservatism of the K- and CTOD-concepts is caused due to

* the CTOD linear extrapolation from the crack flank to the crack tip
* the CTOD and K_I determination from conservative specimens (constraint) tending towards the plane strain condition at the crack tip
* the conservative conversion of K_{IJ} values from J.

The evaluation of the constraint indicated higher deformation reserves for the area of the nozzle corner under internal pressure and thermal shock loading.

References

/1/ HDR-Sicherheitsprogramm, Gesamtprogramm, Phase I, Rev. 4, Stand Januar 1982

/2/ Kußmaul, K., "Beanspruchungs- und Versagensuntersuchungen an Druckbehälter und Rohrleitungen", 7. Statusbericht, HDR-Programm, Karlsruhe, Dezember 1983

/3/ Jansky, J., Krolop, S., Stegmeyer, R., Pfeffer, P., Deuster, G., Brinette, R., "Pressurized thermal shock loading at nozzle corner area of HDR-RPV", ASME-RPV Conference, San Antonio, Texas, June 1984

/4/ Jansky, J., Bhongbhibhat, T., "Spannungsuntersuchungen an Druckbehälterstutzen bei Blowdownbelastung", KfK Karlsruhe, TWB Nr. 51-84, Juli 1984

/5/ Jansky, J., Blind, D., Katzenmeier, G., "Erkenntnisse aus einem Rohrabriß an der HDR-Versuchsanlage unter Betriebsbedingungen mit Einfluß von hohem Sauerstoffgehalt", 10. MPA-Seminar, Stuttgart, Oktober 1984

/6/ Schmitt, W., Blauel, J.G., Hodulak, M.,Jansky, J., "Rißfortschrittsrechnungen (3D-FE) für die Stutzenkante des RDB bei Thermoschock und erster Vergleich mit Versuchsergebnissen", 8. Statusbericht, HDR-Programm, Karlsruhe, Dezember 1984

/7/ Maydowski, R., Kygowitzer, P.J., Speidel, M.O., "The effect of crack branching on the residual lifetime of steam turbines containing stress corrosion cracks", Dechema-Conference, European Federation of Corrosion, München, September 1984

/8/ Blind, D., Jansky, J., Müller, K.U., Diem, H., Fischer, H., "MPA-Dokumentation und Interpretation des HDR-Rundabrisses", MPA-Vorlage zur RSK-Sitzung vom 21.3.1984, Stuttgart, März 1984

/9/ Irwin, G.R., Structural aspect of brittle fracture, Appl. Mat. Res., 65, 1964

/10/ Krägeloh, E., "Bruchmechanik - werkstoffmechanisch betrachtet, VGB Kraftwerkstechnik, 61. Jahrgang, Heft 9, 1981, pp. 782-799

/11/ Bickel, Ruiz, "Pressure vessel design and analysis, Pergamon - Press, 1971

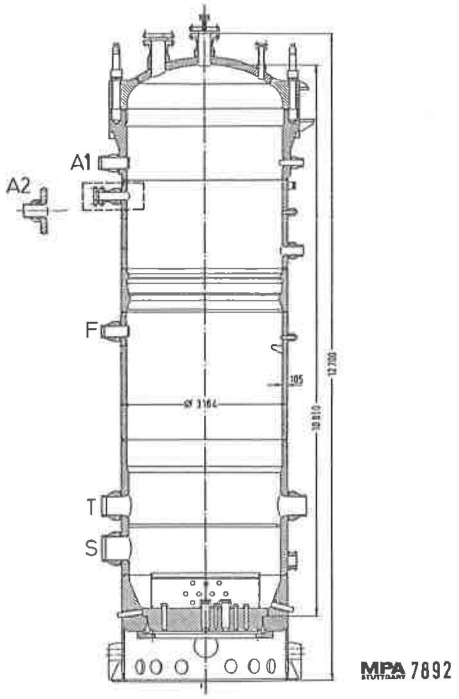

Fig. 1: HDR-RPV geometrical data

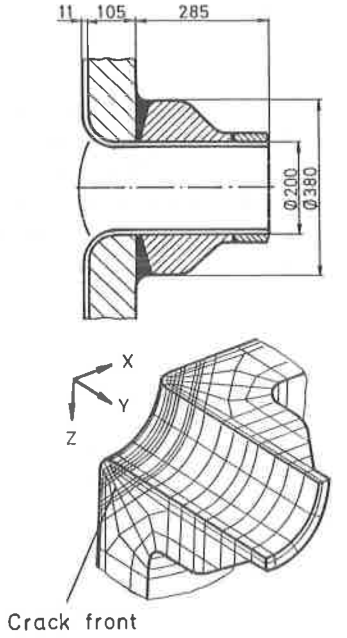

Fig. 2: Geometrical data for nozzle A2, with a FE-modell idealisation

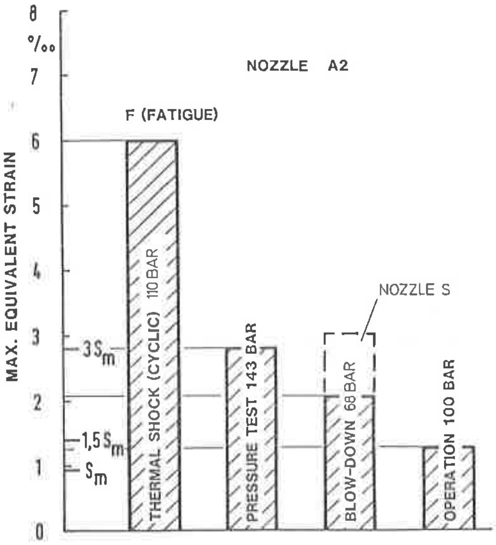

Fig. 3: Calculated equivalent strains for different loading in the A2-nozzle

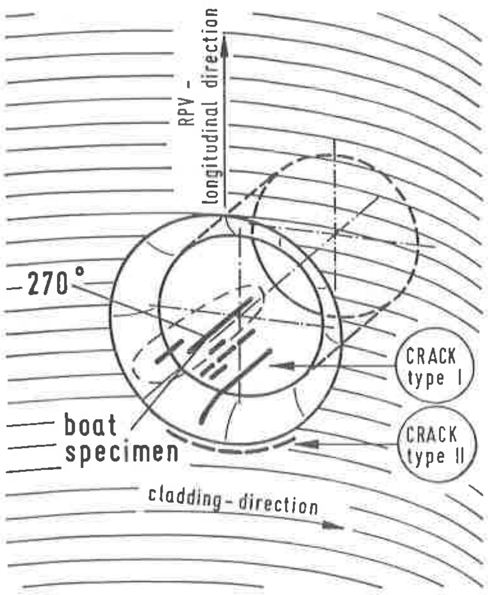

Fig. 4: Incipient cracking in A2-nozzle and position of boat specimen cutted-out for fractographic examination

FIG 1/4*

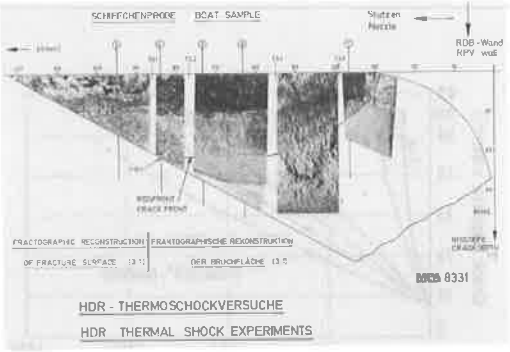

Fig. 5: Fractographic reconstruction of boat specimen fracture surface

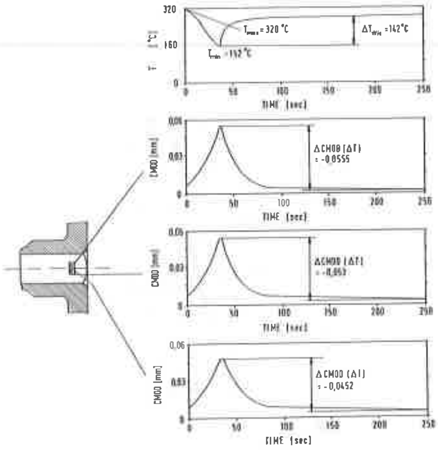

Fig. 6: CMOD-measurements on nozzle A2-longitudinal crack at 270°-position during blow-down loading

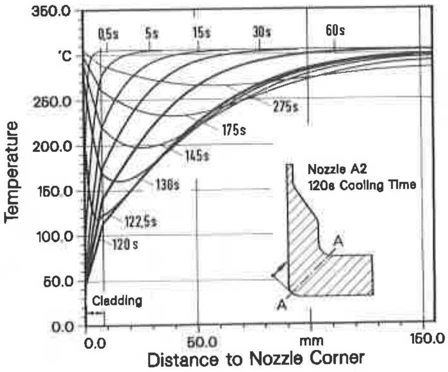

Fig. 7: Calculated temperature distribution in the A2-nozzle wall due to 120 s long thermal shock and during reheating time

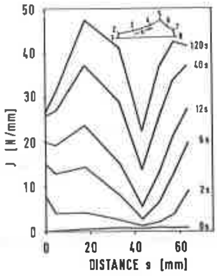

Fig. 8: Calculated crack tip loading J during 120 s cooling time

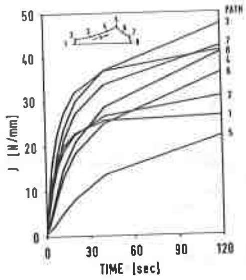

Fig. 9: Time dependant loading J in different depth along the crack tip

F1G 1/4*

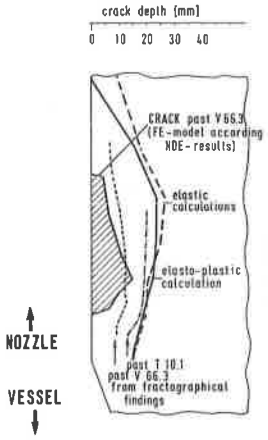

Fig. 10: Comparison of theoretically calculated and fractographically estimated crack geometries at different thermal shock test stages

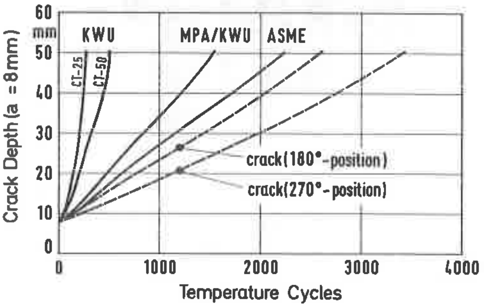

Fig. 11: Calculated crack extension during thermal shock test as a function of different material tests results

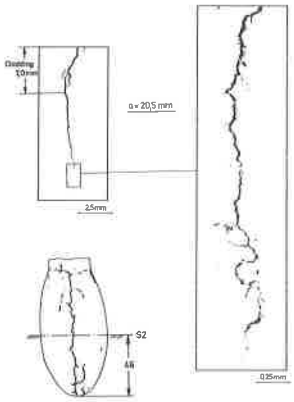

Fig. 12: Crack branching documentated in metallographical cut of examinated boat specimen

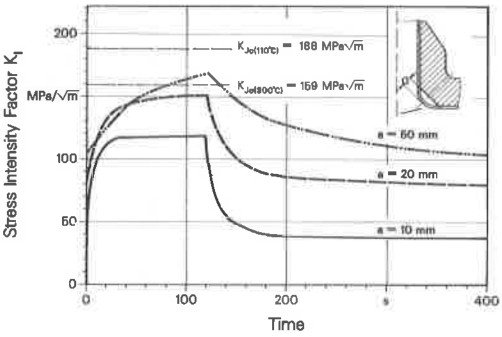

Fig. 13: Elastically calculated K_I -values compared with K_{IJ} material constants estimated by elasto-plastic testing

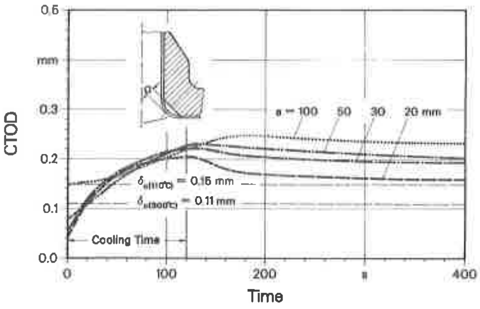

Fig. 14: Elasto-plastically calculated CTOD-values compared with δ_{cr} from elasto-plastic material tests

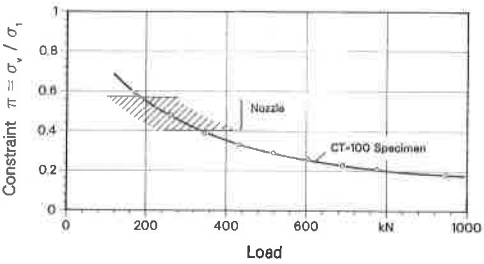

Fig. 15: Comparison between the constraint of CT-100 specimen with a constraint in the A2-nozzle during the thermal shock test